Nonlinear Control of a DC MicroGrid for the Integration of Photovoltaic Panels

Alessio Iovine, Sabah Benamane Siad, Gilney Damm, *Member, IEEE*, Elena De Santis, *Senior Member, IEEE*, and Maria Domenica Di Benedetto, *Fellow, IEEE*

***Abstract*— New connection constraints for the power network (grid codes) require more flexible and reliable systems, with robust solutions to cope with uncertainties and intermittence from renewable energy sources (renewables), such as photovoltaic (PV) arrays. The interconnection of such renewables with storage systems through a direct current (DC) MicroGrid can fulfill these requirements. A "Plug and Play" approach based on the "System of Systems" philosophy using distributed control methodologies is developed in this paper. This approach allows to interconnect a number of elements to a DC MicroGrid as power sources, such as PV arrays, storage systems in different time scales, such as batteries and supercapacitors, and loads, such as electric vehicles and the main ac grid. The proposed scheme can easily be scalable to a much larger number of elements.**

***Note to Practitioners*—Renewable energy can play a key role in producing local, clean, and inexhaustible energy to supply the world's increasing demand for electricity. Photovoltaic (PV) conversion of solar energy is a promising solution and is the best fit in several situations. However, its intermittent nature remains a real difficulty that can create instability. To answer to the new constraints of connection to the network (grid codes) for either solar plant than distributed generation, one possible solution is the use of direct current (DC) MicroGrids, including storage systems, in order to integrate the electric power generated by these PV arrays. One of the main reasons is the fact that PV panels, batteries, supercapacitors, and electric vehicles are DC. On the other hand, reliable stable control of DC MicroGrids is still an open problem. In particular, it lacks rigorous analysis that can establish the operation regions and stability conditions for such MicroGrids. Current works that consider realistic grids usually apply from-the-shelf solutions that do not study the dynamics of such grids. While more rigorous studies just consider too much simplified grids that do not represent the conditions from real life applications, this paper presents nonlinear controllers capable to stabilize the DC MicroGrid, with rigorous analysis on the sufficient conditions and region of operation of the proposed control.**

***Index Terms*— Direct current (DC) MicroGrid, DC power systems, Lyapunov methods, photovoltaic (PV) power systems, power generation control.**

Manuscript received September 25, 2016; revised December 18, 2016; accepted January 10, 2017. Date of publication March 17, 2017; date of current version April 5, 2017. This paper was recommended for publication by Associate Editor A. Pashkevich and Editor S. Grammatico upon evaluation of the reviewers' comments. *(Corresponding author: Alessio Iovine.)*

A. Iovine, E. De Santis, and M. D. Di Benedetto are with the Center of Excellence DEWS and also with the Department of Information Engineering, Computer Science and Mathematics, University of L'Aquila, 67100 L'Aquila, Italy (e-mail: alessio.iovine@univaq.it; elena.desantis@univaq.it; mariadomenica.dibenedetto@univaq.it).

S. B. Siad and G. Damm are with Laboratoire IBISC - Informatique, Biologie Intégrative et Systèmes Complexes, Paris-Saclay University, 91000 Evry, France (e-mail: sabah.siad-benamane@ibisc.fr; gilney.damm@ibisc.fr).

Color versions of one or more of the figures in this paper are available online at http://ieeexplore.ieee.org.

Digital Object Identifier 10.1109/TASE.2017.2662742

I. Introduction

RENEWABLE energy can play a key role in producing local, clean, and inexhaustible energy to supply the world's increasing demand for electricity. Photovoltaic (PV) conversion of solar energy is a promising way to meet the growing demand for energy, and is the best fit in several situations [1]. However, its intermittent nature remains a real disability that can create voltage (or even frequency in the case of islanded MicroGrids) instability for large-scale grids. In order to answer to the new constraints of connection to the network (grid codes), it is possible to consider storage devices [2], [3]; the whole system will be able to inject the electric power generated by PV panels to the grid in a controlled and efficient way. As a consequence, it is necessary to develop a strategy for managing energy in relation to the load and the storages constraints. Direct current (DC) microgrids are attracting interest thanks to their ability to easily integrate modern loads, renewables sources, and energy storages [4]–[8], since most of them (such as electric vehicles, batteries, and PV panels) are naturally DC; therefore, in this paper, a DC microgrid composed by a source, a load, two storages working in different time scales, and their connecting devices is considered.

The utilized approach is based on a "Plug and Play" philosophy: the global control will be carried out at local level by each actuator, according to distributed control paradigm. The controller is developed in a distributed way for stabilizing each part of the whole system, while performing power management in real time to satisfy the production objectives while assuring the stability of the interconnection to the main grid.

Even if control techniques for converters are a well-known research field [9]–[12], the models generally used are obtained by the linearization of average models around an operation region. These linearized models are based on some assumptions, with several implications. First of all, they assume to have full controllability of the system [13], [14]; in reality, due to technical reasons, systems have an additional variable (a capacitor) on the source side [15]. Controlling this capacitor implies that another variable (the grid side capacitor) is uncontrolled; this remaining dynamics is usually neglected by the assumption that it is connected (and implicitly stabilized) by an always stable strong main grid. Removing this assumption to consider a realistic grid implies that this dynamics needs to be considered when studying grid stability. An additional consideration of the use of linearized models around an equilibrium point is that the linearization hides

the nonlinear interconnection of the networked system. For this reason, either the chosen equilibrium point is stable or is not stable without further analysis. As will be shown in the following, when considering the nonlinear model, it can be seen that the stability of such systems is much more complex needing more complex control schemes. Such controllers trade this increase of complexity for assuring stability inside a whole operation region.

A second characteristics of this paper is that most literature of MicroGrids focuses on higher level controllers [16], [17]. Such works assume that local controllers are applied to each converter, and are composed of nested proportional–integrals (PIs) (commonly called vectorial control or control of current and voltage loops). Such linear controllers cannot counteract the networked nonlinearities that may lead the system to instability (or at least to an oscillatory behavior), and can only stabilize the system inside a small operation region. These were some of the main motivations for using a more complete nonlinear model of the converters, and to focus on the local controllers.

To the best of our knowledge, no rigorous nonlinear stability analysis has been developed for a realistic model of a DC MicroGrid. In this paper, convergence analysis is performed for the full dynamics composing the grid. In the same way, dynamics interaction is evaluated in order to obtain voltage stability in the DC MicroGrid in response to load and generation variations. Indeed, as introduced in this paper, only a rigorous analysis of all the dynamics provides the grid stability conditions to assure this stability.

The adopted control strategy is shown to work both in case of time-varying uncontrolled load than in case of constant controlled load; both problems being relevant [18], [19]. The whole system provides protection against faults and suppresses interference, and has a positive impact on the behavior of the complete electrical system. The final management system can be configurable and adaptable as needed.

This paper is organized as follows. In Section III, the model of the DC MicroGrid is introduced. Then, in Section IV, the adopted control laws for each subsystem are proved to satisfy stability requirements. Section V provides simulation results about the connected system behavior, while in Section VI the conclusions are provided.

II. Problem Definition

The reference framework is shown in Fig. 1, where the isolated DC microgrid is represented. The targets would be to assure voltage DC grid stability while correctly feeding the load. To each element (PV array, battery and supercapacitor), a DC/DC converter is connected; their dynamical models are described in Section III.

The whole control objective is then split into several tasks; the first one is to extract the maximum available power from the PV array. This maximum power production is obtained calculating the optimal value of the duty cycle in order to fix the PV array connected capacitor voltage to a given reference. Backstepping theory is used to stabilize the DC/DC boost converter that connects the solar array to the DC network.

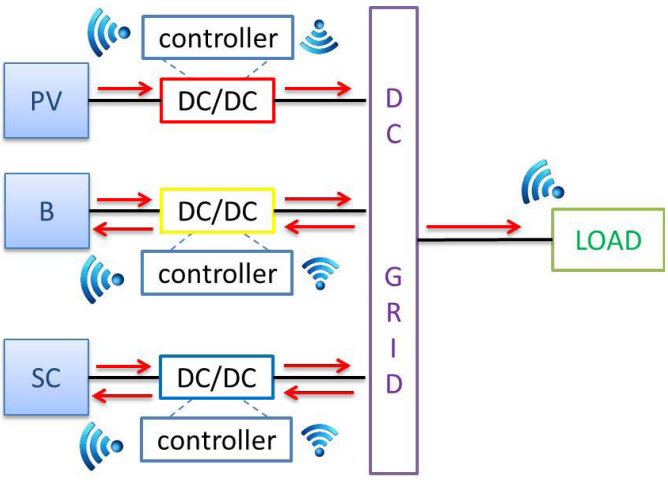

Fig. 1. Considered framework.

The focus then moves to the storage systems and their connection to the DC network. In this paper, two kinds of storage are considered: a battery, which purpose is to provide/absorb the power when needed, and a supercapacitor, which purpose is to stabilize the DC grid voltage in case of disturbances. DC/DC bidirectional converters are necessary to enable the two modes of functioning (charge and discharge). The battery is assimilated as a reservoir, which acts as a buffer between the flow requested by the network and the flow supplied by the production sources, and its voltage is controlled by the DC/DC current converter. Again, backstepping theory is used for designing the controller and assuring stability. With this structure, the DC grid is able to provide a continuous supply of good quality energy.

The three converters present in this system must, in a distributed way, keep the stability of the DC network interconnecting all parts. The final management system can be configurable and adaptable as needed.

In this paper, all the considered dynamics are supposed to be measurable. Furthermore, all the model parameters (the values of resistances, capacitances, and inductances) are known.

A. Assumptions

In this paper, two main assumptions are made: the first one is the existence of a higher level controller, which provide references to be accomplished by the local controllers [20]; the second one is about a proper sizing of each component of the microgrid in order to have feasible power balance.

1) Higher Level Controller: The power output coming from the sources needs to be properly coordinated and controlled. Here, we assume that a higher level controller provides references for the local controllers; these references change every fixed time interval T and concern the amount of power needed for the next time interval and the desired voltage value for the DC grid. The time interval T is decided by the high level controller according to the computational time needed for calculations. These references are about the desired voltage to impose to the PV array and to the battery to obtain the needed amount of power, V_1^* and V_4^*, respectively, and the desired voltage value for the DC grid, V_9^*. We need the references to be able to consider a proper charge/discharge rate power for the

supercapacitor; a state of charge about 50% of its operability at the beginning of the time interval is the best starting point for efficiency reasons.

2) Energy Balance: Proper sizing of each component in a DC microgrid is an important feasibility requirement. In order to always satisfy the power demanded by the load, the sizing of the PV array, battery, and supercapacitor fit some conditions related to the P_{PV} produced power by the PV array, the P_B and P_{SC} stored power into the battery and the supercapacitor, respectively, and the P_L power absorbed by the load.

1) The sizing of the PV array is performed according to total energy needed into a whole day
$$\int_0^D P_{\mathrm{PV}}\, dt \geq \int_0^D P_L\, dt \tag{1}$$
where D is equal to daytime, 24 h.
2) The sizing of the battery and the supercapacitor is performed according to the energy balance in a T time step, needed for selecting a new reference
$$\left\| \int_{kT}^{(k+1)T} (P_{\mathrm{PV}} + P_B - P_L)\, dt \right\| \leq \frac{1}{2} \int_{kT}^{(k+1)T} P_{\mathrm{SC}}\, dt \quad \forall\, k. \tag{2}$$

The last condition can be seen as the ability of the supercapacitor to fulfill the request to provide enough amount of power in the considered time interval; for sizing the supercapacitor we consider the worst scenario due to current load variations, i.e., the case where the supercapacitor needs to provide/absorb the maximum available current for all the time step.

The complete sizing of these components is considered out of the scope at this point, and will be studied in the future works.

III. DC MicroGrid Modeling

In this section, the considered framework shown in Fig. 1 is described. The PV array, battery and supercapacitor are each one connected to the DC grid by a DC/DC converter. Here, the circuital representation and the mathematical model are given, based on power electronics averaging technique [21], [22] controlled using Pulse Width Modulation [23]

$$\dot{x}(t) = f(x(t)) + g(x(t), u(t), d(t)) + h(x(t), d(t)) \tag{3}$$
$$x = [x_1\ x_2\ x_3\ x_4\ x_5\ x_6\ x_7\ x_8\ x_9\ ]^T \tag{4}$$
$$u = [u_1\ \ u_2\ \ u_3\ ]^T \tag{5}$$
$$d = \left[V_{\mathrm{PV}}\ \ V_B\ \ V_S\ \ \frac{1}{R_L} \right]^T. \tag{6}$$

The state $x \in \mathbb{R}^9$ and the disturbance vector $d \in \mathbb{R}^4$ are supposed to be measurable. Here, x_9 represents the voltage $V_{C_9} : \mathbb{R} \to \mathbb{R}^+$ of the capacitor C_9, which is the DC microgrid (shown in violet in Fig. 2). Such voltage is influenced by the connections with load and sources: $R_L \in \mathbb{R}^+$ is a constant value representing the load resistance, while the positive values of R_2, R_5, and R_7 are the resistances among the dynamics x_9 and the interconnected dynamics x_2, x_5, and x_7. These dynamics are the voltages $V_{C_2} : \mathbb{R} \to \mathbb{R}^+$, $V_{C_5} : \mathbb{R} \to \mathbb{R}^+$, and $V_{C_7} : \mathbb{R} \to \mathbb{R}^+$ of the capacitors C_2, C_5, and C_7, which are components of the three DC/DC converters connected, respectively, to the PV array (red area), the battery (yellow area), and the supercapacitor (blue area) shown in Fig. 2. Their description is introduced in the following:

$$\begin{cases}
\dot{x}_1 = -\dfrac{1}{R_1 C_1} x_1 - \dfrac{1}{C_1} x_3 + \dfrac{1}{R_1 C_1} V_{\mathrm{PV}} \\
\dot{x}_2 = -\dfrac{1}{R_2 C_2} x_2 + \dfrac{1}{C_2} x_3 - \dfrac{1}{C_2} u_1 x_3 + \dfrac{1}{R_2 C_2} x_9 \\
\dot{x}_3 = \dfrac{1}{L_3} [x_1 - x_2 - R_{01} x_3] \\
\qquad + \dfrac{1}{L_3} (x_2 + (R_{01} - R_{02}) x_3) u_1 \\
\dot{x}_4 = -\dfrac{1}{R_4 C_4} x_4 - \dfrac{1}{C_4} x_6 + \dfrac{1}{R_4 C_4} V_B \\
\dot{x}_5 = -\dfrac{1}{R_5 C_5} x_5 + \dfrac{1}{C_5} x_6 - \dfrac{1}{C_5} u_2 x_6 + \dfrac{1}{R_5 C_5} x_9 \\
\dot{x}_6 = \dfrac{1}{L_6} x_4 - \dfrac{1}{L_6} x_5 - \dfrac{R_{04}}{L_6} x_6 + \dfrac{1}{L_6} x_5 u_2 \\
\dot{x}_7 = -\dfrac{1}{R_7 C_7} x_7 + \dfrac{1}{C_7} x_8 + \dfrac{1}{R_7 C_7} x_9 \\
\dot{x}_8 = \dfrac{1}{L_8} V_S u_3 - \dfrac{R_{08}}{L_8} x_8 - \dfrac{1}{L_8} x_7 \\
\dot{x}_9 = \dfrac{1}{C_9} \left[\dfrac{x_2 - x_9}{R_2} + \dfrac{x_5 - x_9}{R_5} + \dfrac{x_7 - x_9}{R_7} - x_9 \dfrac{1}{R_L} \right].
\end{cases} \tag{7}$$

A. PV Branch

The DC/DC converter needed to connect the PV array to the DC grid is a boost converter: it is illustrated in the red area in Fig. 2. The equivalent circuit representation for the boost converter can be expressed using a state space average model. Three state variables are needed for the system model: the capacitor voltages $V_{C_1} : \mathbb{R} \to \mathbb{R}^+$ and $V_{C_2} : \mathbb{R} \to \mathbb{R}^+$ (x_1 and x_2, respectively) and the inductor current $I_{L_3} : \mathbb{R} \to \mathbb{R}$ (x_3). C_1, C_2, R_1, R_2, L_3, R_{01}, and R_{02} are known positive values of the capacitors, resistances, and the inductor while the disturbance $V_{\mathrm{PV}} \in \mathbb{R}^+$ is the PV panel voltage. The measured signals are the states x_1, x_2, and x_3 and the PV array voltage V_{PV}. u_1 is the control input, which is defined as the duty cycle of the circuit; its target is to properly integrate the power coming from the PV array and at the same time to obtain the maximum amount of power from the solar energy. This is known as the maximum power point tracking (MPPT) and consists to regulate the voltage V_{C_1} to its reference $V_1^* = x_1^*$ given by a higher level controller,

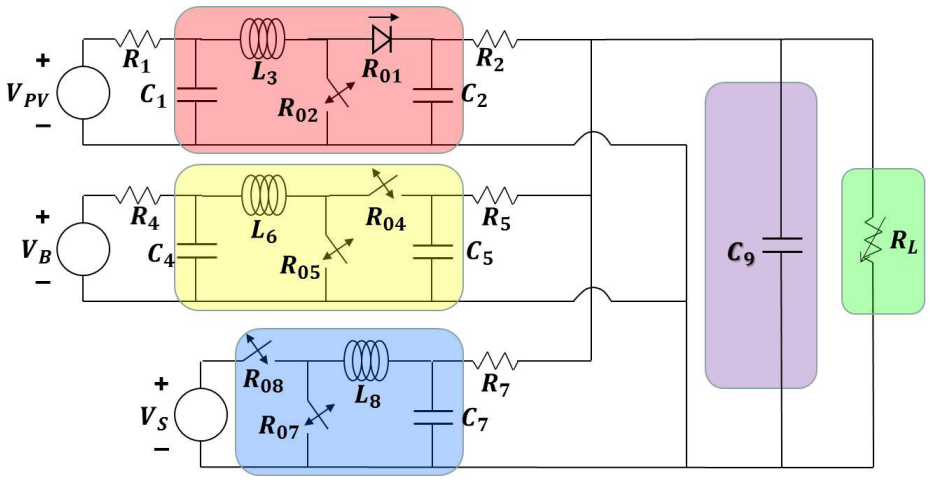

Fig. 2. Interconnected system.

and considered constant during each time interval T. The MPPT is implemented in the higher level controller: it is not a purpose of this paper to describe in detail the MPPT algorithm, which is the standard Incremental Conductance Algorithm well known in the literature.

B. Battery Branch

The DC/DC converter connecting the battery to the DC grid is a bidirectional converter: it is illustrated in the yellow area in Fig. 2. As for the boost converter, we select three state variables: the capacitor voltages $V_{C_4} : \mathbb{R} \to \mathbb{R}^+$ and $V_{C_5} : \mathbb{R} \to \mathbb{R}^+$ (x_4 and x_5, respectively) and the inductor current $I_{L_6} : \mathbb{R} \to \mathbb{R}$ (x_6). C_4, C_5, R_4, R_5, L_6, R_{04}, and R_{05} are known positive values of the circuit while the disturbance $V_B \in \mathbb{R}^+$ is the battery voltage. The measured signals are the states x_4, x_5, and x_6 and the battery voltage V_B. The duty cycle u_2 is the control input; its target is to assign the reference $V_4^* = x_4^*$ value to x_4, forcing the battery to provide/absorb a desired amount of power, in a smooth way that maximizes its lifetime. This reference value is given by a higher controller not considered in this present paper, and is considered as constant during the time period T.

Remark 1: It must to be noticed that the reference in terms of voltage x_4^* has the same meaning as a reference in terms of power. Indeed, the output voltage of the battery is a function of the state of charge, which is a function of the battery current as well. The secondary controller provides a reference about the power P_B that must come out from the battery branch; it is translated in the reference V_4^* in steady state. We can write the power P_B as $P_B = I_B * V_{DC}$, where V_{DC} is the voltage of the grid and I_B is the battery current. Being P_B given and V_{DC} known, we can calculate the needed I_B as a function of V_{C_4}.

C. Supercapacitor Branch

The DC/DC converter connecting the supercapacitor to the DC grid is a buck one.[1] Only two state variables are needed, x_7 for the capacitor voltage $V_{C_7} : \mathbb{R} \to \mathbb{R}^+$ and x_8 for the inductor current $I_{L_8} : \mathbb{R} \to \mathbb{R}$. The positive values of C_7, R_7, L_8, R_{07}, and R_{08}, and the disturbance $V_S : \mathbb{R} \to \mathbb{R}^+$ (supercapacitor voltage) are known at each t. The model describing the evolution of the supercapacitor voltage is taken as in [24]. The duty cycle u_3 is the control input for this system. Its target is to control the capacitor voltage directly connected to the grid, which is x_7. The measured signals are the states x_7 and x_8, and the supercapacitor voltage $V_S(t) > 0$.

Remark 2: According to the supercapacitors target to maintain voltage grid stability, the supercapacitor is not expected to be completely charged or discharged. As stated in Section II-A2, the high level controller is supposed to calculate the reference for the power coming from the battery in a way such that the supercapacitors state of charge is 50% of its operability (about 75% of maximum voltage) at the beginning of each time interval (this is the best starting point for efficiency reasons) without considering unmodeled disturbances. So the voltage is kept at a level that is the minimum level demanded by the application (the level of the DC grid plus the converters minimum ratio) plus the voltage needed to let the supercapacitors state of charge vary of 50% of the remaining energy (close to 75% of maximum voltage). Finally, since energy is $E = (1/2)CV_{\mathrm{SC}}^2$, if voltage reaches 50% of maximum voltage, remaining energy is 25% of maximum energy. Driving voltage further down reduces lifetime with very small gain of available power.

IV. Grid Control

In this section, control laws are derived to fit the desired targets: for each DC/DC converter, a proper control action is developed and the interconnection among all of them is then used to ensure grid stability. Let us consider the state x, whose dynamics are described in (7). Let us consider the set of all possible values of x_1^* that generate a nonnegative current coming from the PV array as $x_1^* \in [\gamma_1 V_{\mathrm{PV}}, V_{\mathrm{PV}}]$, where $\gamma_1 = (R_{01}/R_1)(1/1 + (R_{01}/R_1))$. Given a positive value of R_L and x_9^*, let us moreover consider the set of all positive values of

[1]The converter used for the supercapacitor has different constraints from the one used for the battery, and for this reason is of a different topology.

x_4^* such that the balance of the currents is expressed by

$$\frac{1}{R_L}x_9^* = \frac{1}{R_2}\left(x_2^* - x_9^*\right) + \frac{1}{R_5}\left(x_5^* - x_9^*\right) \tag{8}$$

where the values of x_2^* and x_5^* depend on x_1^* and x_4^*, respectively, and are defined as

$$x_2^* = \frac{x_9^* - a_2}{2} + \frac{1}{2}\sqrt{\left(x_9^* - a_2\right)^2 + 4R_2C_2\left(\Delta_2 + a_2x_9^*\right)} \tag{9}$$

$$\Delta_2 = \frac{1}{R_1C_2}\left(V_{\mathrm{PV}} - x_1^*\right)\left[x_1^* - \frac{R_{02}}{R_1}\left(V_{\mathrm{PV}} - x_1^*\right)\right] \tag{10}$$

$$a_2 = \frac{R_{01} - R_{02}}{R_1}\left(V_{\mathrm{PV}} - x_1^*\right) \tag{11}$$

$$x_5^* = \frac{x_9^*}{2} + \frac{1}{2}\sqrt{x_9^{*2} + 4R_5C_5\Delta_5} \tag{12}$$

$$\Delta_5 = \frac{1}{R_4C_5}(V_B - x_4^*)\left[x_4^* - \frac{R_{04}}{R_4}(V_B - x_4^*)\right] \tag{13}$$

and represent the solution of the dynamics x_2 and x_5 in (7) setting $\dot{x} = 0$.

Theorem 1: For any given $x_1^* \in [\gamma_1 V_{\mathrm{PV}}, V_{\mathrm{PV}}]$, $x_9^* > 0$, and $x_4^* > 0$, such that condition (8) is satisfied, consider the point x_e

$$x^e = \begin{bmatrix} x_1^e \\ x_2^e \\ x_3^e \\ x_4^e \\ x_5^e \\ x_6^e \\ x_7^e \\ x_8^e \\ x_9^e \end{bmatrix} = \begin{bmatrix} x_1^* \\ x_2^* \\ \frac{1}{R_1}\left(V_{\mathrm{PV}} - x_1^*\right) \\ x_4^* \\ x_5^* \\ \frac{1}{R_4}\left(V_B - x_4^*\right) \\ x_9^* \\ 0 \\ x_9^* \end{bmatrix}. \tag{14}$$

There exist control laws u_1, u_2, and u_3, such that x^e is the equilibrium point for the closed loop system in (7) and any evolution of (7) satisfying for each t the conditions

$$x_2 + (R_{01} - R_{02})x_3 \neq 0, \quad x_5 \neq 0, \quad x_9 \neq 0 \tag{15}$$

asymptotically converges to x^e.

Proof: The proof is based on the use of a Lyapunov function V, which is a composition of different Lyapunov functions, as illustrated in [25] and [26]. We use PI control inputs u_1 and u_2 for properly controlling dynamics x_1, x_3, x_4, and x_6 in order to obtain a desired amount of power coming from the PV array and the battery. Then, the control input u_3 focuses on the grid voltage regulating the interconnection among the systems. The control laws are developed by using a backstepping technique. The proposed Lyapunov function is

$$V = V_{1,3} + V_{4,6} + V_7 + V_8 + V_{2,5,9} \tag{16}$$

where all the terms are defined as follows.

Let us first focus on the control u_1, which is dedicated to dynamics x_1 and x_3: it is defined as

$$u_1 = \frac{1}{x_2 + (R_{01} - R_{02})x_3}[-x_1 + x_2 + R_{01}x_3 - L_3\upsilon_1] \tag{17}$$

with

$$\upsilon_1 = K_3(x_3 - z_3) + \overline{K}_3\alpha_3 - C_1\overline{K}_1K_1^{\alpha}\left(x_1 - x_1^*\right) + \left(C_1K_1 - \frac{1}{R_1}\right)\left(K_1(x_1 - x_1^*) + \overline{K}_1\alpha_1\right) \tag{18}$$

$$z_3 = \frac{1}{R_1}\left(V_{\mathrm{PV}} - x_1\right) + C_1K_1\left(x_1 - x_1^*\right) + C_1\overline{K}_1\alpha_1 \tag{19}$$

where the positive gains K_3, $\overline{K}_3$, K_3^{α}, $\overline{K}_1$, K_1^{α}, and K_1, have to be properly chosen, and α_1 and α_3 are integral terms assuring zero error in steady state

$$\dot{\alpha}_1 = K_1^{\alpha}\left(x_1 - x_1^*\right) \quad \dot{\alpha}_3 = K_3^{\alpha}\left(x_3 - z_3\right). \tag{20}$$

An augmented system can be considered for the dynamics x_1 and x_3, where the state, the disturbance vector, and the relating matrices are

$$\bar{x}_{1,3} = [x_1 \ \alpha_1 \ x_3 \ \alpha_3]^T \tag{21}$$

$$\bar{d}_{1,3} = \left[V_{\mathrm{PV}} \ x_1^*\right]^T \tag{22}$$

$$\dot{\bar{x}}_{1,3} = A_{1,3}\bar{x}_{1,3} + D_{1,3}\bar{d}_{1,3} \tag{23}$$

$$A_{1,3} = \begin{bmatrix} -\frac{1}{R_1C_1} & 0 & -\frac{1}{C_1} & 0 \\ K_1^{\alpha} & 0 & 0 & 0 \\ a_{31} & a_{32} & -K_3 & -\overline{K}_3 \\ K_3^{\alpha}\left(\frac{1}{R_1} - C_1K_1\right) & -K_3^{\alpha}C_1\overline{K}_1 & K_3^{\alpha} & 0 \end{bmatrix} \tag{24}$$

$$a_{31} = (K_3 - K_1)\left(C_1K_1 - \frac{1}{R_1}\right) + C_1\overline{K}_1K_1^{\alpha} \tag{25}$$

$$a_{32} = \overline{K}_1\left(K_3C_1 - K_1C_1 + \frac{1}{R_1}\right) \tag{26}$$

$$D_{1,3} = \begin{bmatrix} \frac{1}{R_1C_1} & 0 \\ 0 & -K_1^{\alpha} \\ \frac{K_3}{R_1} & d_{32} \\ -\frac{K_3^{\alpha}}{R_1} & C_1K_1K_3^{\alpha} \end{bmatrix} \tag{27}$$

$$d_{32} = -C_1\overline{K}_1K_1^{\alpha} + K_1\left(C_1K_1 - K_3C_1 - \frac{1}{R_1}\right). \tag{28}$$

System (23) has the following equilibrium point:

$$\bar{x}_{1,3}^e = \begin{bmatrix} x_1^* & 0 & \frac{V_{\mathrm{PV}} - x_1^*}{R_1} & 0 \end{bmatrix}^T. \tag{29}$$

The characteristic polynomial is considered; to obtain stability, all the terms need to be strictly positive, i.e., $p_3 > 0$, $p_2 > 0$,

TABLE I
ROUTH TABLE

1	p_2	p_0
p_3	p_1	0
$p_2 - \frac{p_1}{p_3}$	$p_o p_1 \frac{1}{p_3}$	
$p_2 - p_0 p_1 \frac{1}{p_2 - \frac{p_1}{p_3}}$		

$p_1 > 0,\ p_0 > 0$

$$p(\lambda) = \lambda^4 + p_3\lambda^3 + p_2\lambda^2 + p_1\lambda + p_0 \tag{30}$$

$$p_3 = K_3 + \frac{1}{R_1 C_1} > 0 \tag{31}$$

$$p_2 = \overline{K}_3 K_3^{\alpha} + \frac{1}{R_1 C_1} K_3 + \overline{K}_1 K_1^{\alpha} + \left[(K_3 - K_1)\left(K_1 - \frac{1}{R_1 C_1} \right) \right] > 0 \tag{32}$$

$$p_1 = \frac{1}{R_1 C_1}(\overline{K}_3 K_3^{\alpha} + \overline{K}_1 K_1^{\alpha}) + \overline{K}_1 K_1^{\alpha}(K_3 - K_1) + K_3^{\alpha}\left(K_1 - \frac{1}{R_1 C_1} \right) > 0 \tag{33}$$

$$p_0 = \overline{K}_1 \overline{K}_3 K_3^{\alpha} K_1^{\alpha} > 0. \tag{34}$$

Due to the hypothesis of positive gains, conditions (31) and (34) are always satisfied; furthermore, $K_3 > K_1$ and $K_1 > (1/R_1C_1)$ are sufficient conditions for (32) and (33) to be respected. Other conditions are given by the Routh criterium in Table I

$$p_2 > \frac{p_1}{p_3}, \quad p_2 - \frac{p_0 p_1}{p_2 - \frac{p_1}{p_3}} > 0. \tag{35}$$

It can be shown that these conditions can be fulfilled with a proper choice of the parameter K_3. We do not include here the corresponding calculations for lack of space. As a result, an asymptotically stable linear system is obtained; then, there will exist a Lyapunov function $V_{1,3}$ in the form of

$$V_{1,3} = \frac{1}{2}\left(\bar{x}_{1,3} - \bar{x}_{1,3}^e\right)^T P_{1,3}\left(\bar{x}_{1,3} - \bar{x}_{1,3}^e\right) > 0 \tag{36}$$

with

$$\dot{V}_{1,3} < 0 \tag{37}$$

where the symmetric positive definite matrix $P_{1,3}$ is obtained by the Lyapunov equation $A_{1,3}^T P_{1,3} + P_{1,3} A_{1,3} = -Q_{1,3}$, such that (37) is verified.

The control input u_2, which is dedicated to control the dynamics x_4 and x_6 and to ensure a desired charge/discharge behavior of the battery imposing the reference x_4^*, is of the form of

$$u_2 = \frac{1}{x_5}(-x_4 + x_5 + R_{04} x_6 + L_6 v_2) \tag{38}$$

with

$$v_2 = -K_6(x_6 - z_6) - \overline{K}_6 \alpha_6 + \overline{K}_4 K_4^{\alpha}\left(x_4 - x_4^*\right) - \left(C_4 K_4 - \frac{1}{R_4} \right)\left(K_4(x_4 - x_4^*) + \overline{K}_4 \alpha_4 \right) \tag{39}$$

where the positive gains K_6, $\overline{K}_6$, K_6^{α}, $\overline{K}_4$, K_4^{α}, and K_4 are properly chosen and

$$z_6 = \left(\frac{1}{R_4}(V_B - x_4) + C_4 K_4(x_4 - x_4^*) + C_4 \overline{K}_4 \alpha_4 \right) \tag{40}$$

$$\dot{\alpha}_4 = K_4^{\alpha}\left(x_4 - x_4^*\right) \quad \dot{\alpha}_6 = K_6^{\alpha}(x_6 - z_6) \tag{41}$$

with α_4 and α_6 being integral terms assuring zero error in steady state.

As for the previous case, an augmented system can be considered

$$\dot{\bar{x}}_{4,6} = A_{4,6}\bar{x}_{4,6} + D_{4,6}\bar{d}_{4,6} \tag{42}$$

$$\bar{x}_{4,6} = [\ x_4\ \ \alpha_4\ \ x_6\ \ \alpha_6\ ]^T \tag{43}$$

$$\bar{d}_{4,6} = [\ V_B\ \ x_4^*\ ]^T. \tag{44}$$

The system in (42) has matrices $A_{4,6}$ and $D_{4,6}$ similar to $A_{1,3}$ and $D_{1,3}$ in (23), with respect to the considered gains. Also, similar to (29), system (42) has the following equilibrium point:

$$\bar{x}_{4,6}^e = \left[x_4^*\ \ 0\ \ \frac{V_B - x_4^*}{R_4}\ \ 0\ \right]^T. \tag{45}$$

The same considerations drive to the same asymptotic stability result; then, there will exist a Lyapunov function $V_{4,6}$ in the form of

$$V_{4,6} = \frac{1}{2}\left(\bar{x}_{4,6} - \bar{x}_{4,6}^e\right)^T P_{4,6}\left(\bar{x}_{4,6} - \bar{x}_{4,6}^e\right) > 0 \tag{46}$$

with

$$\dot{V}_{4,6} < 0 \tag{47}$$

where the symmetric positive definite matrix $P_{4,6}$ is obtained by the Lyapunov equation $A_{4,6}^T P_{4,6} + P_{4,6} A_{4,6} = -Q_{4,6}$, such that (47) is verified.

Let us now focus on the control input u_3, which is determined to ensure voltage grid stability. It does not act directly on the DC grid, but through the dynamics x_8 and x_7. Utilizing backstepping and Lyapunov methods, we can select the desired value for the dynamics to control the grid. The Lyapunov functions provided at each step will be used for the entire system, thereby leading to the study of composite Lyapunov functions.

The function $V_{2,5,9}$ refers to dynamics x_2, x_5, and x_9; introducing the errors e_2 and e_5 between the dynamics and their equilibrium points as

$$e_2 = x_2 - x_2^*, \quad e_5 = x_5 - x_5^*$$

we can rewrite the equations as

$$\begin{cases} \dot{e}_2 = \dfrac{1}{R_2 C_2}\left(x_9 - e_2 - x_2^*\right) + \dfrac{1}{C_2} x_3(1 - u_1) \\ \dot{e}_5 = \dfrac{1}{R_5 C_5}\left(x_9 - e_5 - x_5^*\right) + \dfrac{1}{C_5} x_6(1 - u_2) \\ \dot{x}_9 = \dfrac{1}{C_9}\left(\dfrac{1}{R_2}\left(e_2 + x_2^* - x_9\right) + \dfrac{1}{R_5}\left(e_5 + x_5^* - x_9\right) \right) \\ + \dfrac{1}{C_9}\left(\dfrac{1}{R_7}(x_7 - x_9) - \dfrac{1}{R_L} x_9 \right). \end{cases} \tag{48}$$

To find a proper controller, $V_{2,5,9}$ can be defined as

$$V_{2,5,9} = \frac{C_2}{2} e_2^2 + \frac{C_5}{2} e_5^2 + \frac{C_9}{2} x_9^2. \tag{49}$$

Then

$$\begin{aligned}\dot{V}_{2,5,9} = &-\frac{1}{R_2}e_2^2 + e_2\left(\frac{1}{R_2}\left(x_9 - x_2^*\right) + x_3(1-u_1)\right)\\ &-\frac{1}{R_5}e_5^2 + e_5\left(\frac{1}{R_5}\left(x_9 - x_5^*\right) + x_6(1-u_2)\right)\\ &+x_9\left(\frac{1}{R_2}\left(e_2 + x_2^* - x_9\right) + \frac{1}{R_5}\left(e_5 + x_5^* - x_9\right)\right)\\ &+x_9\left(\frac{1}{R_7}(x_7 - x_9) - \frac{1}{R_L}x_9\right). \end{aligned} \tag{50}$$

In (50), the dynamics x_7 can be seen as control input; it can be properly chosen to obtain a desired form for $\dot{V}_{2,5,9}$. By choosing the value z_7 for x_7 as

$$\begin{aligned} z_7 = &-R_7\frac{1}{x_9}\left[e_2\left(\frac{1}{R_2}\left(x_9 - x_2^*\right) + x_3(1-u_1)\right)\right]\\ &-R_7\frac{1}{x_9}\left[e_5\left(\frac{1}{R_5}\left(x_9 - x_5^*\right) + x_6(1-u_2)\right)\right]\\ &+R_7\left[\frac{x_9}{R_L} - \frac{1}{R_2}\left(e_2 + x_2^* - x_9\right) - \frac{1}{R_5}\left(e_5 + x_5^* - x_9\right)\right]\\ &+\frac{1}{x_9}\left(-x_9^{*2} + 2x_9x_9^*\right). \end{aligned} \tag{51}$$

$\dot{V}_{2,5,9}$ results to be semidefinite negative. To prove asymptotic stability, the set Ω is considered: it is the largest invariant set of the set E of all points where the Lyapunov function is not decreasing. Ω contains a unique point; then, applying LaSalle's theorem asymptotic stability of the equilibrium point can be established

$$\dot{V}_{2,5,9} = -\frac{1}{R_2}e_2^2 - \frac{1}{R_5}e_5^2 - \frac{1}{R_7}(x_9 - x_9^*)^2 \le 0 \tag{52}$$

$$\begin{aligned}\Omega &= \{(e_2, e_5, x_9):\ x_2 = x_2^*,\ x_5 = x_5^*,\ x_9 = x_9^*\}\\ &= \{(0, 0, x_9^*)\}. \end{aligned} \tag{53}$$

In order to calculate $z_8(t)$, such that x_8 steps back the value of x_7 to the desired value z_7, we use the Lyapunov function

$$V_7 = \frac{1}{2}(x_7 - z_7)^2 \tag{54}$$

where the desired dynamics for x_7 is

$$\dot{x}_7 = -K_7(x_7 - z_7) \tag{55}$$

with a gain $K_7 > 0$. By Lyapunov function time derivative calculation, we obtain the reference z_8

$$z_8 = -C_7K_7(x_7 - z_7) + \frac{1}{R_7}(x_7 - x_9) + C_7\dot{z}_7. \tag{56}$$

Indeed, the Lyapunov derivative is negative definite if the value of x_8 is properly chosen as z_8 in (56)

$$\begin{aligned}\dot{V}_7 &= (x_7 - z_7)(\dot{x}_7 - \dot{z}_7)\\ &= (x_7 - z_7)\left(-\frac{1}{R_7C_7}x_7 + \frac{1}{C_7}x_8 + \frac{1}{R_7C_7}x_9 - \dot{z}_7\right) \end{aligned} \tag{57}$$

$$\dot{V}_7 = -K_7(x_7 - z_7)^2 < 0. \tag{58}$$

To calculate the control input u_3, we again use backstepping technique: we can obtain it by using the Lyapunov function

$$V_8 = \frac{1}{2}(x_8 - z_8)^2 \tag{59}$$

whose time derivative is

$$\begin{aligned}\dot{V}_8 &= (x_8 - z_8)(\dot{x}_8 - \dot{z}_8)\\ &= (x_8 - z_8)\left(\frac{1}{L_8}V_S u_3 - \frac{R_{08}}{L_8}x_8 - \frac{1}{L_8}x_7 - \dot{z}_8\right). \end{aligned} \tag{60}$$

To have a negative definite $\dot{V}_8$, the control input must be

$$u_3 = \tfrac{1}{V_S}[x_7 + R_{08}x_8 + L_8\dot{z}_8 - L_8K_8(x_8 - z_8)] \tag{61}$$

with $K_8 > 0$ and constant

$$\dot{z}_8 = -C_7K_7(\dot{x}_7 + \dot{z}_7) + \frac{1}{R_7}(\dot{x}_7 - \dot{x}_9) + C_7\ddot{z}_7 \tag{62}$$

and where the function $\ddot{z}_7$ is the time derivative of $\dot{z}_7$

$$\dot{V}_8 = (x_8 - z_8)(\dot{x}_8 - \dot{z}_8) = -K_8(x_8 - z_8)^2 < 0. \tag{63}$$

Then, using the control laws defined in (17), (38), and (61), in accordance with (36), (46), (49), (54), and (59), we have positive definite Lyapunov functions $V_{1,3} > 0$, $V_{4,6} > 0$, $V_{2,5,9} > 0$, $V_7 > 0$, and $V_8 > 0$, such that their time derivatives $\dot{V}_{1,3} < 0$, $\dot{V}_{4,6} < 0$, $\dot{V}_{2,5,9} \le 0$, $\dot{V}_7 < 0$, and $\dot{V}_8 < 0$ ensure stability, according to (37), (47), (52), (58), and (63).

The composite positive definite Lyapunov function V in (16) results to have a negative semidefinite time derivative $\dot{V}$; LaSalle's theorem ensures asymptotic stability of the equilibrium x^e of the entire system describing the DC microgrid

$$\dot{V} = \dot{V}_{1,3} + \dot{V}_{4,6} + \dot{V}_7 + \dot{V}_8 + \dot{V}_{2,5,9} \le 0. \tag{64}$$

□

As proved in Theorem 1, the uncontrained control laws u_1, u_2, and u_3 solve our problem. When considering a realistic application, control laws must be bounded: $u_1 \in [0, 1]$, $u_2 \in [0, 1]$ and $u_3 \in [0, 1]$. These bounds also impose limitations for x_1^*, x_4^*, and x_9^*. Bounds on x_1^* have already been considered in the theorem to have a current coming from the PV array. A bounded u_2 imposes bounds on x_9^*, $x_9^* \in (\max(V_{\mathrm{PV}}, V_B), V_S)$, and on x_4^*, $x_4^* \in [\gamma_2 V_B, \beta(x_9^*, V_B)]$, where $\gamma_2 = (R_{04}/R_4)(1/1 + (R_{04}/R_4))$ and

$$\beta(x_9^*, V_B) = \frac{x_9^* + \left(\frac{R_5}{R_4} - \frac{R_{04}}{R_4}\right)V_B}{1 + \frac{R_5}{R_4} - \frac{R_{04}}{R_4}}. \tag{65}$$

When considering the bounds $u_1 \in [0, 1]$ and $u_2 \in [0, 1]$, bounds on the resistance R_L must be satisfied as well: indeed, given the $x_9^* \in (\max(V_{\mathrm{PV}}, V_B), V_S)$, only the values of $R_L \in \Omega_{R_L}$, where

$$\begin{aligned}\Omega_{R_L} = \big\{&R_L : x_4^* \in \left[\gamma_2 V_B, \beta\left(x_9^*, V_B\right)\right]\\ &\text{for some } x_1^* \in [\gamma_1 V_{\mathrm{PV}}, V_{\mathrm{PV}}]\big\} \end{aligned} \tag{66}$$

is the set, such that condition (8) is satisfied with respect to physical limitations of all the components of the circuits.

Let $X = \mathbb{R}^{13}$ be the state space of the closed loop system. Given the state feedback control laws $u_1 : X \to \mathbb{R}$, $u_2 : X \to \mathbb{R}$, and $u_3 : X \to \mathbb{R}$, in (17), (38), and (61), for any value of the used gains, we need to compute the maximal set

$$\Omega_K \subset X \tag{67}$$

TABLE II
RATINGS

Branch	Rating
PV	1 MW
Battery	1 MW
Supercapacitor	0.5 MW
Load	1 MW
Grid nominalvoltage	1000 V

which is invariant for the closed loop dynamical system, and is such that $u_1(z) \in [0, 1]$, $u_2(z) \in [0, 1]$, and $u_3(z) \in [0, 1]$, $\forall z \in \Omega_K$. Such a maximal set is well defined, because the family of all invariant set in X is closed under union. We can prove that the set Ω_K is not empty.

Theorem 2: For any $R_L \in \Omega_{R_L}$, for any $x_1^* \in [\gamma_1 V_{\mathrm{PV}}, V_{\mathrm{PV}}]$, such that $x_4^* \in [\gamma_2 V_B, \beta(x_9^*, V_B)]$, for any x_9^*, such that $\max(V_{\mathrm{PV}}, V_B) < x_9^* < V_S$, there exist gains K_1, $\overline{K}_1$, K_1^α, K_3, $\overline{K}_3$, K_3^α, K_4, $\overline{K}_4$, K_4^α, K_6, $\overline{K}_6$, K_6^α, K_7, and K_8, such that $\Omega_K \neq \emptyset$.

Proof: To prove controller existence, without loss of generality, let us now consider the controllers u_1 and u_2 where no integral error correction terms are considered: the value of the gains $\overline{K}_1$, K_1^α, $\overline{K}_3$, K_3^α, $\overline{K}_4$, K_4^α, $\overline{K}_6$, K_6^α is set to be zero. As we are neglecting the integral error dynamics, stability conditions to be respected are stated only by the formulas in (31) and (32). A choice of K_1 and K_3 (K_4 and K_6) respecting these conditions is done: $K_1 = (1/R_1C_1)$ and $K_3 = (R_{01}/L_3)$ ($K_4 = (1/R_4C_4)$ and $K_6 = (R_{04}/L_6)$). A simple choice of K_7 and K_8 respecting stability is $K_7 = (1/R_7C_7)$ and $K_8 = (R_{08}/L_8)$. The conditions $x_1^* \in [\gamma_1 V_{\mathrm{PV}}, V_{\mathrm{PV}}]$, $x_4^* \in [\gamma_2 V_B, \beta(x_9^*, V_B)]$, $R_L \in \Omega_{R_L}$, and $\max(V_{\mathrm{PV}}, V_B) < x_9^* < V_S$ imply that x^e is an equilibrium with $u_1(x^e) \in [0, 1]$, $u_2(x^e) \in [0, 1]$, and $u_3(x^e) \in [0, 1]$. Therefore, $x^e \in \Omega_K$. The same can be done including the integral terms. □

It is not easy to determine Ω_K analytically, but an estimation of Ω_K can be obtained, for example, by following the method proposed in [27]. Considering a sufficiently small neighborhood of the equilibrium point x_e, and the gains $\overline{K}_1$, K_1^α, $\overline{K}_3$, K_3^α, $\overline{K}_4$, K_4^α, $\overline{K}_6$, and K_6^α, backward reachability analysis can be used to compute the states starting from which the evolutions reach that neighborhood in finite time (and therefore converge to the equilibrium point) with bounded inputs. Such evolutions will automatically satisfy condition (15).

Corollary 1: For any given $R_L \in \Omega_{R_L}$, $\forall\ x_1^* \in [\gamma_1 V_{\mathrm{PV}}, V_{\mathrm{PV}}]$: $x_4^* \in [\gamma_2 V_B, \beta(x_9^*, V_B)]$, $\forall\ x_9^*$, such that $max(V_{\mathrm{PV}}, V_B) < x_9^* < V_S$, given the state feedback control laws u_1, u_2, and u_3, defined in (17), (38), and (61), and for any initial state in Ω_K, the state $z(t)$ of the closed loop system asymptotically converges to x^e, and $u_1(z(t)) \in [0, 1]$, $u_2(z(t)) \in [0, 1]$, and $u_3(z(t)) \in [0, 1]$, $\forall t \geq 0$.

V. Simulation Results

In this section, we present some simulations that show the results obtained using the proposed control inputs. Such simulations are obtained using MATLAB. The values of the parameters for the model are depicted in Tables II and III.

The simulation target is to correctly feed a load and to maintain the grid stability, which means to ensure no large variation in the DC grid voltage. The simulation time is 20 s. The considered reference value x_9^* for the DC grid voltage is selected as $x_9^* = 1000$ V. A secondary controller is supposed to provide the references to be reached in each time interval; during that period, the introduced control laws will bring the devices to operate in the desired points. The selected strategy assigns to the PV and battery the duty to fulfill the losses into the network; the references will then be calculated according to the load current. The references are updated every second: during the first 10 s, the load is supposed to be constant during each time interval of a second.

TABLE III
GRID PARAMETERS

Parameter	Value	Parameter	Value
C_1	0.1 F	L_3	0.033 H
C_2	0.01 F	R_{01}	0.01 Ω
R_1	0.1 Ω	R_{02}	0.01 Ω
R_2	0.1 Ω	C_4	0.1 F
C_5	0.01 F	R_{04}	0.01 Ω
R_4	0.1 Ω	R_{05}	0.01 Ω
R_5	0.01 Ω	L_6	0.033 H
C_7	0.01 F	L_8	0.0033 H
R_{07}	0.01 Ω	R_{08}	0.01 Ω
R_7	0.1 Ω	C_9	0.0001 F

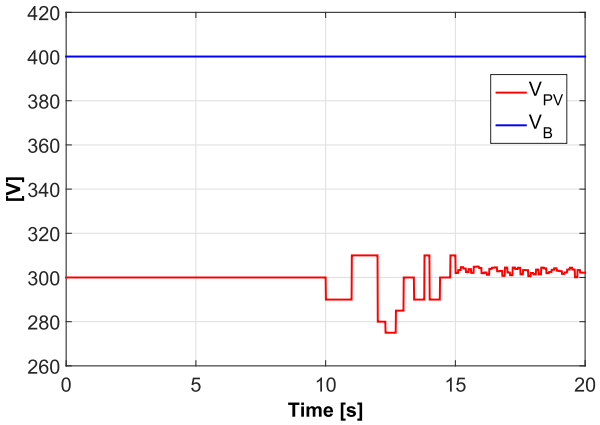

Fig. 3. Voltages of V_{PV} (red line) and V_B (blue line).

A. Nonlinear Control

We can split the simulation in two parts: in the first one, from 0 to 10 s, the voltages of the PV array and of the battery are constant and the load resistance piecewise constant. Furthermore, the references provided by the higher level controller are exact and the supercapacitor is needed only for providing grid stability during the transient time needed by the converters that are connected to the PV and the battery. In the second part of the simulation, in addition to the step variation, the load is supposed to be time-varying and disturbances acting on the PV voltage are considered (see Fig. 3). To better represent any possible case, we have also simulated the case where the references do not fulfill the energy balance: there the supercapacitor will need to provide power during all the time window. Fig. 4 describes the values of the conductance $(1/R_L)$ over the time; we can see the described behavior, which is piecewise constant for 10 s and then becomes time-varying.

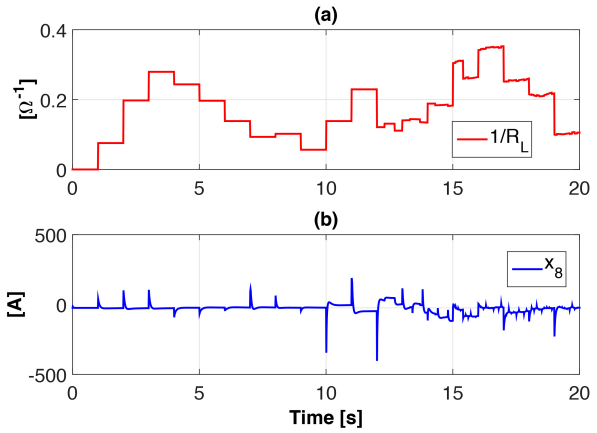

Fig. 4. (a) Load conductance $(1/R_L)$. (b) Current x_8 when implementing the introduced nonlinear control.

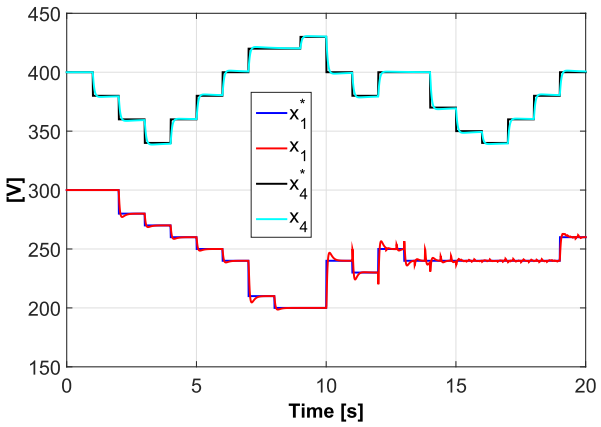

Fig. 5. Voltages of C_1 (red line) and C_4 (cyan line) following the desired references, and the blue and black lines, respectively, when implementing the introduced nonlinear control.

In accordance to the values of $(1/R_L)$, the references x_1^* and x_4^* are obtained for the power balance target. As shown in Fig. 5, the C_1 and C_4 capacitor voltages reach the desired values during the considered time step. Here, two different situations for the controllers are faced, because the two devices need two different treatments; we need from the PV array to start providing the highest level of power as soon as possible, while the battery needs to have a smooth behavior to preserve its lifetime. The integral terms in the control action are introduced in Figs. 6 and 7; the considered eigenvalues for the systems are different because of the different targets. We note that both the charge and discharge battery situations are faced. Here, we considered the voltage of the battery not to be affected by the current behavior; indeed, a constant value is used to represent it, because the battery is supposed to be sized in such a way that it is not affected by current dynamics over a time of 20 s. The resulting voltage dynamics on the grid connected capacitors, C_2 and C_5, are modified by the current flow generated by the sources; all the dynamics are stable, as shown in Fig. 8. Their evolution is influenced by the value of the DC grid voltage, which is the capacitor C_9: its value over time is shown in Fig. 9. To satisfy stability constraints, in response to the load variations and to the missing power coming from the PV and the battery, the voltage of the capacitor C_7 reacts balancing the energy variation.

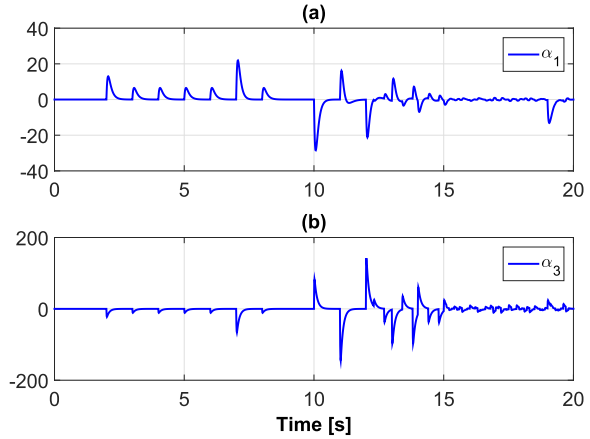

Fig. 6. Integral terms used by the control law u_1 in (17). (a) α_1. (b) α_3.

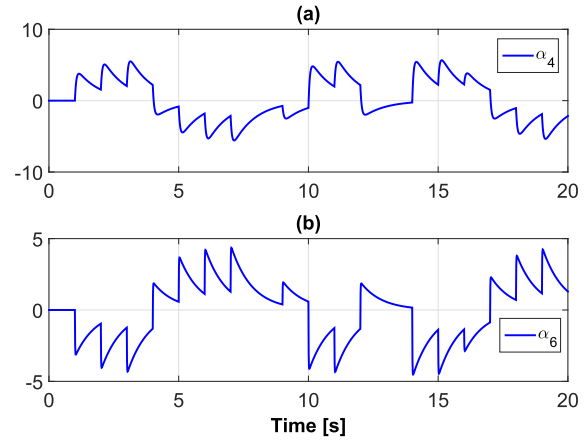

Fig. 7. Integral terms used by the control law u_2 in (38). (a) α_4. (b) α_6.

Fig. 10 describes the currents generated from the PV and the battery: these dynamics are dependent on the voltages and related to them. Fig. 11 introduces the generated control inputs u_1 and u_2, that are bounded by the devices to be between zero and one, while Fig. 3 shows the voltages of the PV array and of the battery. The control inputs are smooth except in the case of reference step variations. The control input for the DC/DC converter connected to the supercapacitor is shown in Fig. 12: its variation depends on the variations of voltage V_S (see Fig. 13) and of the load (see Fig. 4). As results, the desired voltage for the DC microgrid is always kept (Fig. 9). The developed control strategy is then shown to successfully operate in a wide range of situations: constant and time-varying load, acting of perturbation on the sources and big step variations of the references.

B. Comparison With Vectorial Control

Nowadays, the most common utilized technique for controlling converters is composed of nested PIs, and called vectorial control [8], [13], [16]; however, recently, the advantages of model-based nonlinear control technique like the one introduced in this paper start to be considered [9], [11], [14]. Here, a comparison between the adopted nonlinear control law and the classic PI technique is described.

In Fig. 14, the voltages of C_7 and C_9 are depicted when implementing PI control on the supercapacitor connected

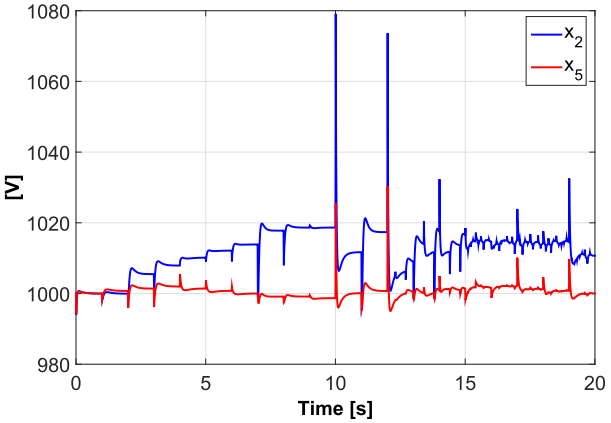

Fig. 8. Voltages of C_2 (blue line) and C_5 (red line) when implementing the introduced nonlinear control.

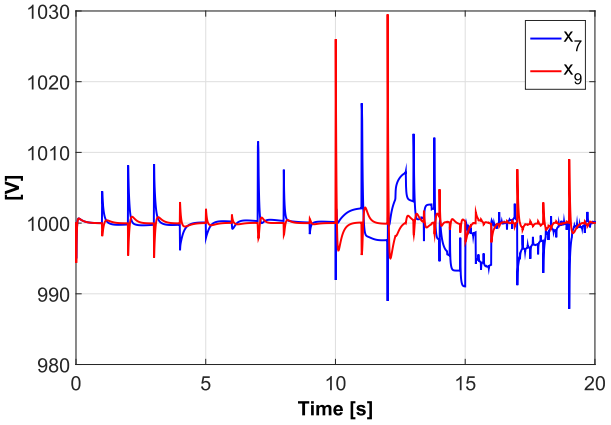

Fig. 9. Voltages of C_7 (blue line) and C_9 (red line) when implementing the introduced nonlinear control.

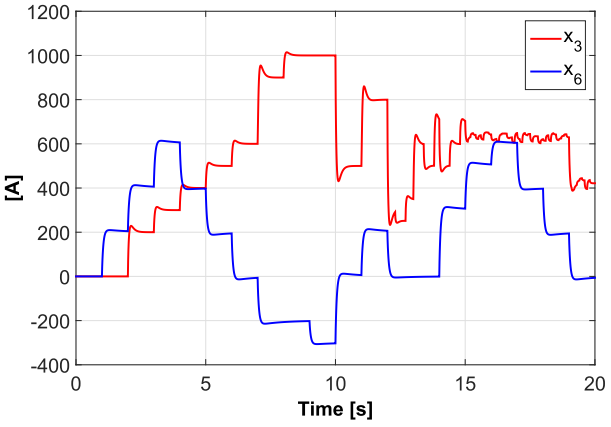

Fig. 10. Currents x_3 (red line) and x_6 (blue line) when implementing the introduced nonlinear control.

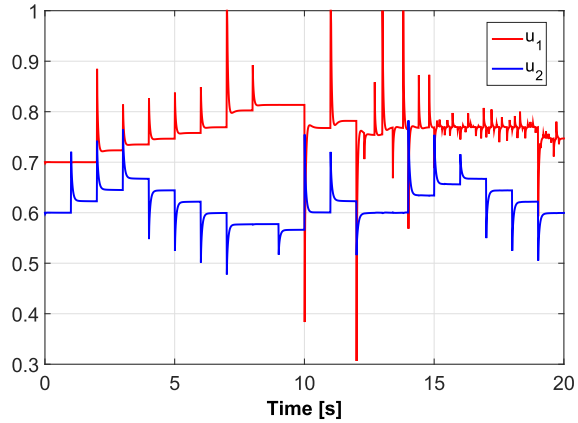

Fig. 11. Control inputs u_1 (red line) and u_2 (blue line) introduced in (17) and (38).

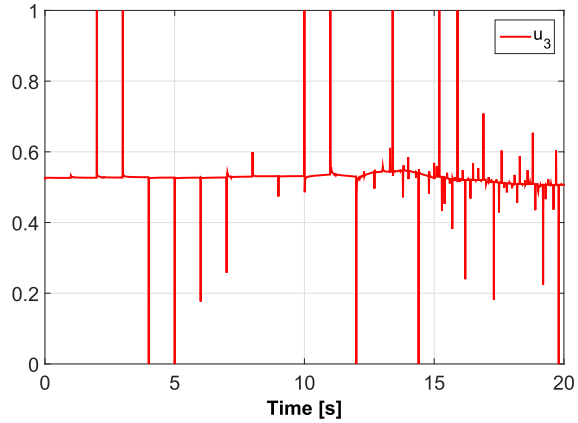

Fig. 12. Control input u_3 in (61).

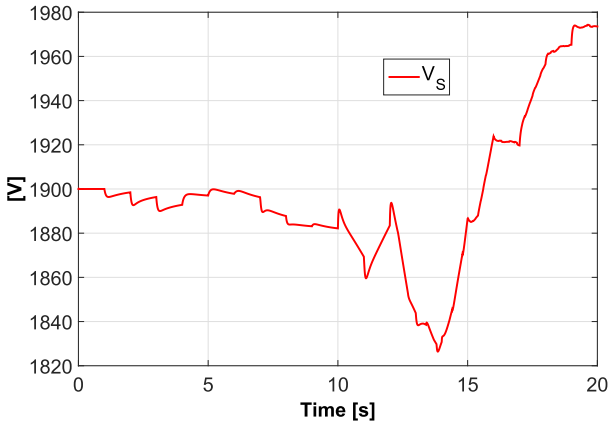

Fig. 13. Voltage of the supercapacitor when implementing the introduced nonlinear control.

DC/DC converter. More in detail, Fig. 15 compares the different behaviors of the voltage of the capacitor representing the DC grid. More variations from the reference value of 1000 V both in steady state that in transient time can be observed when the PI controller is implemented, as well as higher peaks.

The nonlinear control law has then a better behavior, in general, but especially when nonlinearities take place, as a step change or the coupling effects of the disturbances acting on the PV and the load from time 10 to 20 s. Indeed, the PI control is not able to immediately counteract to these phenomena, as shown by the resulting control law u_3 in Fig. 16, which is smoother than the one in Fig. 12. As a result, as can be seen in Fig. 15, the DC grid voltage when using the nonlinear controller keeps closer to the nominal one, and behaves smoother than when controlled by the PIs.

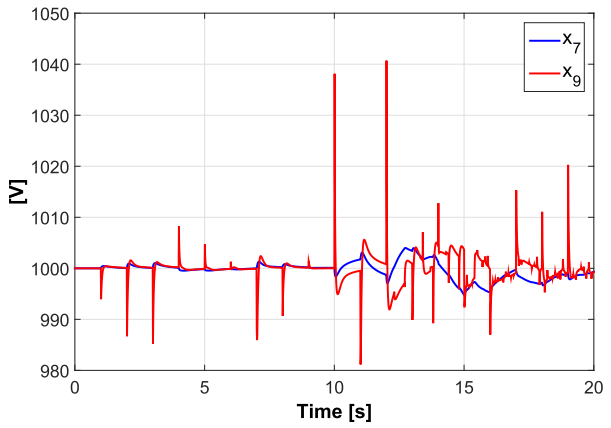

Fig. 14. Voltages of C_7 (blue line) and C_9 (red line) when using PI control.

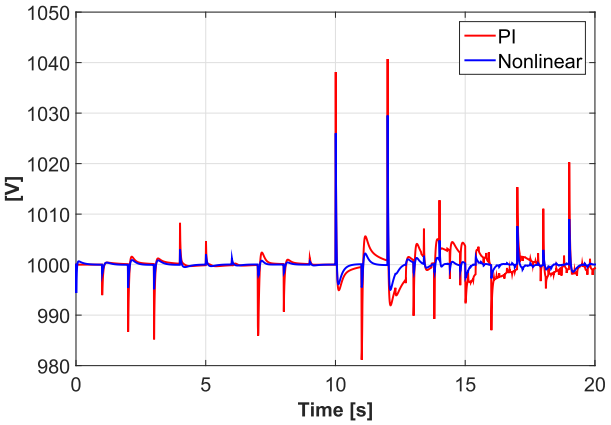

Fig. 15. Comparison on the DC grid dynamics when the converter in charge to control it is controlled by simple PI (red curve) or by the adopted nonlinear technique (blue curve).

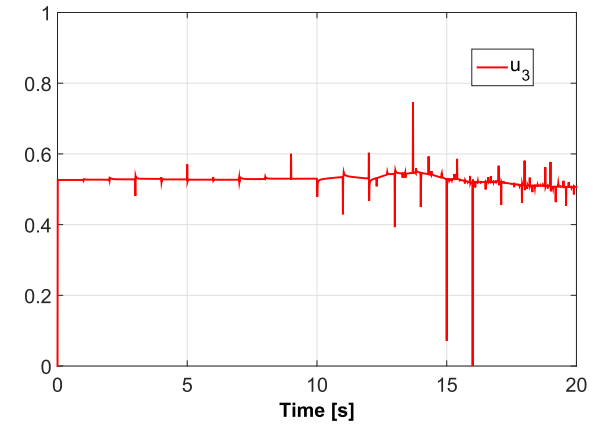

Fig. 16. Control input u_3 when implementing PI control.

The price for this more performing controller is the needed exchange of information among the devices and some model-based calculations. More in detail, the main difficulties arise from the calculation of (62) to be used in (61) and its implementation. However, since the control is a state function, it can be analytically calculated with dedicated tools and implemented.

VI. Conclusion

In this paper, a realistic DC MicroGrid composed by a PV array, two storage devices, a load, and their connected devices is modeled. It is controlled in order to correctly provide a desired amount of power for feeding an uncontrolled bounded load while ensuring a desired grid voltage value. Hypotheses on the ad hoc size of the components are done to physically allow the power exchange. Stability analysis is carried out for the complete system, and physical limitations are also considered. Simulations show the robustness of the adopted control action both during the transient and in steady-state operation mode in case of constant or time-varying load. Comparisons with the standard vectorial control are also carried out, illustrating that the nonlinear controller counteracts the quick interconnected disturbances present in such systems, what is not possible for the linear nested PIs composing the vectorial control.

References

[1] M. A. Eltawil and Z. Zhao, "Grid-connected photovoltaic power systems: Technical and potential problems—A review," *Renew. Sustain. Energy Rev.*, vol. 14, no. 1, pp. 112–129, 2010.

[2] J. P. Barton and D. G. Infield, "Energy storage and its use with intermittent renewable energy," *IEEE Trans. Energy Convers.*, vol. 19, no. 2, pp. 441–448, Jun. 2004.

[3] G. Krajačić, N. Duić, Z. Zmijarević, B. V. Mathiesen, A. A. Vučinić, and M. da Graça Carvalho, "Planning for a 100% independent energy system based on smart energy storage for integration of renewables and CO_2 emissions reduction," *Appl. Thermal Eng.*, vol. 31, no. 13, pp. 2073–2083, 2011.

[4] R. H. Lasseter and P. Paigi, "Microgrid: A conceptual solution," in *Proc. IEEE 35th Annu. Power Electron. Specialists Conf. (PESC)*, vol. 6, Jun. 2004, pp. 4285–4290.

[5] P. Piagi and R. H. Lasseter, "Autonomous control of microgrids," in *Proc. IEEE Power Eng. Soc. General Meeting*, Jun. 2006, pp. 1–8.

[6] N. Hatziargyriou, H. Asano, R. Iravani, and C. Marnay, "Microgrids," *IEEE Power Energy Mag.*, vol. 5, no. 4, pp. 78–94, Jul./Aug. 2007.

[7] T. Dragicevic, J. C. Vasquez, J. M. Guerrero, and D. Skrlec, "Advanced LVDC electrical power architectures and microgrids: A step toward a new generation of power distribution networks," *IEEE Electrific. Mag.*, vol. 2, no. 1, pp. 54–65, Mar. 2014.

[8] J. M. Guerrero, P. C. Loh, T.-L. Lee, and M. Chandorkar, "Advanced control architectures for intelligent microgrids—Part II: Power quality, energy storage, and AC/DC microgrids," *IEEE Trans. Ind. Electron.*, vol. 60, no. 4, pp. 1263–1270, Apr. 2013.

[9] H. Sira-Ramírez and R. Silva-Ortigoza, *Control Design Techniques in Power Electronics Devices*. London, U.K.: Springer-Verlag, 2006, doi: 10.1007/1-84628-459-7

[10] S. Mariethoz *et al.*, "Comparison of hybrid control techniques for buck and boost DC-DC converters," *IEEE Trans. Control Syst. Technol.*, vol. 18, no. 5, pp. 1126–1145, Sep. 2010.

[11] Y. Chen, G. Damm, A. Benchaib, and F. Lamnabhi-Lagarrigue, "Multi-time-scale stability analysis and design conditions of a VSC terminal with DC voltage droop control for HVDC networks," in *Proc. 53rd IEEE Conf. Decision Control*, Dec. 2014, pp. 3266–3271.

[12] Y. Chen, G. Damm, A. Benchaib, M. Netto, and F. Lamnabhi-Lagarrigue, "Control induced explicit time-scale separation to attain DC voltage stability for a VSC-HVDC terminal," in *Proc. 19th IFAC World Congr. Int. Fed. Automat. Control (IFAC)*, vol. 19. Cape Town, South Africa, Aug. 2014, pp. 540–545.

[13] A. P. N. Tahim, D. J. Pagano, E. Lenz, and V. Stramosk, "Modeling and stability analysis of islanded DC microgrids under droop control," *IEEE Trans. Power Electron.*, vol. 30, no. 8, pp. 4597–4607, Aug. 2015.

[14] A. Bidram, A. Davoudi, F. L. Lewis, and J. M. Guerrero, "Distributed cooperative secondary control of microgrids using feedback linearization," *IEEE Trans. Power Syst.*, vol. 28, no. 3, pp. 3462–3470, Aug. 2013.

[15] G. R. Walker and P. C. Sernia, "Cascaded DC-DC converter connection of photovoltaic modules," *IEEE Trans. Power Electron.*, vol. 19, no. 4, pp. 1130–1139, Jul. 2004.

[16] J. M. Guerrero, J. C. Vasquez, J. Matas, L. G. de Vicuna, and M. Castilla, "Hierarchical control of droop-controlled AC and DC microgrids—A general approach toward standardization," *IEEE Trans. Ind. Electron.*, vol. 58, no. 1, pp. 158–172, Jan. 2011.
[17] E. Jiménez, M. J. Carrizosa, A. Benchaib, G. Damm, and F. Lamnabhi-Lagarrigue, "A new generalized power flow method for multi connected DC grids," *Int. J. Elect. Power Energy Syst.*, vol. 74, pp. 329–337, Jan. 2016.
[18] D. Marx, P. Magne, B. Nahid-Mobarakeh, S. Pierfederici, and B. Davat, "Large signal stability analysis tools in DC power systems with constant power loads and variable power loads—A review," *IEEE Trans. Power Electron.*, vol. 27, no. 4, pp. 1773–1787, Apr. 2012.
[19] D. Hamache, A. Fayaz, E. Godoy, and C. Karimi, "Stabilization of a DC electrical network via backstepping approach," in *Proc. IEEE 23rd Int. Symp. Ind. Electron. (ISIE)*, Jun. 2014, pp. 242–247.
[20] D. E. Olivares *et al.*, "Trends in microgrid control," *IEEE Trans. Smart Grid*, vol. 5, no. 4, pp. 1905–1919, Jul. 2014.
[21] S. R. Sanders, J. M. Noworolski, X. Z. Liu, and G. C. Verghese, "Generalized averaging method for power conversion circuits," *IEEE Trans. Power Electron.*, vol. 6, no. 2, pp. 251–259, Apr. 1991.
[22] R. D. Middlebrook and S. Ćuk, "A general unified approach to modelling switching-converter power stages," *Int. J. Electron.*, vol. 42, no. 6, pp. 521–550, 1977.
[23] B. Lehman and R. M. Bass, "Switching frequency dependent averaged models for PWM DC-DC converters," *IEEE Trans. Power Electron.*, vol. 11, no. 1, pp. 89–98, Jan. 1996.
[24] D. Lifshitz and G. Weiss, "Optimal control of a capacitor-type energy storage system," *IEEE Trans. Autom. Control*, vol. 60, no. 1, pp. 216–220, Jan. 2015.
[25] P. Kundur, "Definition and classification of power system stability IEEE/CIGRE joint task force on stability terms and definitions," *IEEE Trans. Power Syst.*, vol. 19, no. 3, pp. 1387–1401, May 2004.
[26] P. Kundur, N. J. Balu, and M. G. Lauby, *Power System Stability and Control*. New York, NY, USA: McGraw-Hill, 1994.
[27] I. M. Mitchell, A. M. Bayen, and C. J. Tomlin, "A time-dependent Hamilton–Jacobi formulation of reachable sets for continuous dynamic games," *IEEE Trans. Autom. Control*, vol. 50, no. 7, pp. 947–957, Jul. 2005.
[28] M. B. Camara, H. Gualous, F. Gustin, and A. Berthon, "Design and new control of DC/DC converters to share energy between supercapacitors and batteries in hybrid vehicles," *IEEE Trans. Veh. Technol.*, vol. 57, no. 5, pp. 2721–2735, Sep. 2008.
[29] M. B. Camara, H. Gualous, F. Gustin, A. Berthon, and B. Dakyo, "DC/DC converter design for supercapacitor and battery power management in hybrid vehicle applications—Polynomial control strategy," *IEEE Trans. Ind. Electron.*, vol. 57, no. 2, pp. 587–597, Feb. 2010.

Alessio Iovine received the B.Sc. and M.Sc. degrees in electrical engineering and computer science and the Ph.D. degree in information science and engineering from the University of L'Aquila, L'Aquila, Italy, in 2010, 2012, and 2016, respectively.

He was a Visiting Student at the University of Lund, Lund, Sweden, in 2011, and a Visiting Ph.D. Student at L2S CentraleSupélec, Paris-Saclay University, Paris, France, from 2014 to 2015. He currently holds a Post-Doctoral position at the University of L'Aquila. His research interests focused on analysis and control of nonlinear and hybrid systems over communication networks, with application to energy systems, such as microgrids, and traffic control.

Sabah Benamane Siad received the B.Sc. degree in electrical engineering from the Conservatoire National des Arts et Metiers de Paris, Paris, France, in 2014. She is currently pursuing the Ph.D. degree with Paris-Saclay University, Paris. Her Ph.D. thesis is on nonlinear control applied to renewable energy sources integration in smartgrids.

Her research interests include nonlinear control, renewable energy and in particular photovoltaic systems, energy storage, distributed generation, DC grids, smartgrids, and microgrids.

Gilney Damm (M'10) received the bachelor's degree in electronic engineer and the M.Sc. degree in automatic control from COPPE–Rio de Janeiro Federal University, Rio de Janeiro, Brazil, in 1995 and 1997, respectively, and the Ph.D. degree in 2001 in the control of power systems and the integration of renewable energy sources and the Habilitation Diriger des Recherches degree from Paris-Saclay University, Paris, France, in 2010.

He is currently an Associate Professor with the Paris-Saclay University. Currently, his main research activities are connected to the Institutes for Energy Transition SuperGrid (on large scale high voltage electrical grids) and Efficacity (on MicroGrids and power grids in SmartCities). His current research interests include nonlinear and adaptive control and observers applied to power systems, such as, smartgrids, supergrid, and microgrids. His main applications are in the field of large scale renewable energy integration, multi-terminal HVDC systems, variable speed pumped storage plants, mixed ac/DC microgrids, control of power generators (transient stabilization, frequency and voltage stability), synchronization of power networks, and energy integration in smartcities.

Prof. Damm has been a member of the IFAC Technical Committee TC 6.3 Power and Energy Systems since 2015. He has been an Associate Editor of the *European Journal of Control* since 2010.

Elena De Santis (M'99–SM'06) received the M.Sc. degree (*cum laude*) in electrical engineering from the University of L'Aquila, L'Aquila, Italy, in 1983.

From 1987 to 1998, she was an Assistant Professor with the University of L'Aquila, where she has been teaching optimal control, as an Associate Professor, since 1998. She has published papers in archival journals, conferences proceedings, and book series in analysis control and optimization of constrained and uncertain dynamic systems, dynamic model management for decision support systems, positive systems, dynamic games, hybrid, and switching systems.

Prof. De Santis is a member of the Executive Committe of the Center of Excellence DEWS (architectures and design methodologies for embedded controllers, wireless interconnected and system-on-chip) of the University of L'Aquila. She is a member of the IFAC Technical Committee TC 1.3 on Discrete Event and Hybrid Systems. She received the Outstanding Reviewer Honorable Mention from the Editorial Board of the IEEE TRANSACTIONS ON AUTOMATIC CONTROL in 2004 and 2013. She has been the chair and an organizer of a number of sessions and a member of the program committee in the main international conferences. She is member of the Editorial Board of the *European Journal of Control*.

Maria Domenica Di Benedetto (F'02) received the Dr.-Ing. (*summa cum laude*) degree in electrical engineering and computer science from the University of Roma La Sapienza, Rome, Italy, in 1976, and the Docteur-Ingnieur and Doctorat d'Etat ès Sciences degrees from the Université de Paris-Sud, Orsay, France, in 1981 and 1987, respectively.

Since 1994, she has been a Professor of Automatic Control with the University of L'Aquila, L'Aquila, Italy. Her research interests are centered about the analysis and control of hybrid systems and networked control systems.

Prof. Di Benedetto was an Associate Editor of the IEEE TRANSACTIONS OF AUTOMATIC CONTROL from 1995 to 1999, and an Associate Editor at Large of the IEEE TRANSACTIONS ON AUTOMATIC CONTROL from 2006 to 2009. Since 1995, she has been a Subject Editor of the *International Journal of Robust and Nonlinear Control*. Since 2016, she has been an Associate Editor of the *IFAC Journal Nonlinear Analysis: Hybrid Systems*. She is the PI and Director of the Center of Excellence for Research DEWS "Architectures and Design Methodologies for Embedded Controllers, Wireless Interconnect and System-on-chip" of the University of L'Aquila. She is the Co-Founder and a member of the Governing Board of WEST Aquila S.r.L. Since 2009, she has been the President of the European Embedded Control Institute. Since 2010, she has been a member of the International Advisory Board of the Lund Center for the control of complex engineering systems. Since 2013, she has been the President of the Italian Society of Researchers in Automatic Control.